TECHNICAL MEMORANDUM

592

The representation of non-orographic gravity waves in the IFS Part I: Assessment of the middle atmosphere climate with Rayleigh friction

Andrew Orr and Nils Wedi

Research Department

May 2009

Abstract

The middle atmosphere climate of cycles 32R3 and 33R1 are assessed. The middle atmosphere climate is determined by the dominating processes of radiation, and wave drag arising from the deposition of momentum from the breaking of small-scale non-orographic gravity waves and large-scale planetary waves. In the current ECMWF Integrated Forecast System (IFS), the averaged effect of the non-orographic gravity wave drag is crudely approximated by Rayleigh friction on the zonal flow. Both cycles have a summer polar upper mesosphere warm bias, which suggests a lack of upwelling, and consequently an underestimation of the poleward circulation between the summer and winter hemispheres and downwelling over the winter pole, i.e. that the Rayleigh friction forcing of the mean flow is unrealistically weak and underestimates the required gravity wave drag.

Given realistic descriptions of radiation and planetary waves, the weak downwelling should be associated with excessively cold winter polar stratospheric temperatures. Both cycles show a southern winter polar cold bias. However, 32R3 has a northern winter polar warm bias, while 33R1 has a northern winter cold pole (but not a cold bias), which is consistent with an improvement in its representation of planetary waves, as shown by the good agreement between simulated and observed planetary wave amplitudes. The failure to simulate a northern winter polar cold bias indicates that the radiation scheme is associated with a northern winter warm bias.

There is also a problem with unrealistically large orographic gravity wave drag at the model top, with a consequent strong compensation by the dynamics. This is alleviated by linearly depositing the orographic gravity wave momentum flux at 0.1 hPa between 0.1 hPa and the model top of 0.01 hPa. However, the northern winter temperature structure and general circulation are more realistic if the smoothing is removed. The results indicate a large imbalance at the model top due to orographic gravity wave drag, which warrants further attention.

1. Introduction

The middle atmosphere comprises the stratosphere and the mesosphere, and is dominated by a winter pole to summer pole temperature gradient, formed by strong solar heating at the summer pole and strong radiative cooling at the winter pole. This causes air to rise/sink at the summer/winter poles, forming a poleward circulation between the summer and winter hemispheres. This meridional circulation generates a Coriolis torque which forms an easterly/westerly jet in the summer/winter hemispheres, peaking in velocity at around the stratopause (Andrews et al., 1987). The mean circulation and thermal structure of the middle atmosphere is further modified by the deposition of momentum arising from the breaking or dissipation of vertically propagating small-scale non-orographic gravity waves (i.e. wave drag) in the mesosphere (Holton, 1982, 1983, 2004; Garcia and Solomon, 1985). This drag decelerates the jets, resulting in a further Coriolis torque which strongly modulates the meridional circulation by inducing additional summer pole to winter pole drift, forcing more air upward/downward over the summer/winter poles, which through adiabatic expansion/compression influences the temperature structure down to the lower stratosphere in the polar regions (Garcia and Boville, 1994).

Planetary wave driving in the extratropical stratosphere, for example from Rossby waves, is also important in winter, and particularly northern winter (Andrews et al., 1987; Garcia and Boville, 1994). Observations show that 1) the southern winter lower and middle polar stratosphere temperature is much colder than in the northern winter, 2) the southern winter polar stratopause is much warmer than in the northern winter, and 3) there exists a much stronger reversal of the latitudinal gradient of stratopause temperature in the southern winter mid to high-latitudes than in the northern winter (Kanzawa, 1989). Matsuno and Nakamura (1979) showed that the drag associated with breaking planetary waves causes rising motion (i.e. cooling) in the

upper stratosphere and sinking motion (i.e. warming) in the lower stratosphere, meaning that the stronger/weaker planetary waves of the northern/southern winter are contributing to these observed temperature differences (Kanzawa, 1989). These large-scale waves are predominately produced in the troposphere from orographic forcing (Holton, 2004). Planetary wave driving is less important in the summer hemisphere, as, for example, the quasi-stationary Rossby waves are trapped by the critical layer formed as the mid-latitude westerly tropospheric jet changes sign to stratospheric easterlies (Holton, 2004).

Thus, the realistic simulation of the middle atmosphere circulation and temperature structure is determined by the dominant processes of radiation, planetary wave activity, and the dissipation of small-scale non-orographic gravity waves. In the ECMWF Integrated Forecast System (IFS), planetary wave activity is resolved by the dynamics (i.e. the dissipation of planetary waves can be effectively thought of as resolved drag), whereas radiation is parametrized.

Non-orographic gravity waves (which hereafter are referred to simply as gravity waves) have vertical wavelengths which vary from less than one to tens of km, and horizontal wavelengths which vary from tens to thousands of km (Gardner et al., 1989; Ern et al., 2004), and are thus generally unresolved or under-resolved by the IFS (Hamilton et al., 1995, 1999), and therefore require parametrization. Garcia and Boville (1994) showed that in the absence of gravity wave drag parametrization, sinking at the southern winter polar stratopause was reduced by a factor of two, resulting in middle atmosphere temperatures too close to radiative equilibrium, notably with unrealistically cold winter polar stratosphere temperatures. Hamilton et al. (1995, 1999) showed that in the absence of gravity wave drag parametrization that the size of the winter polar stratosphere cold bias in the 'SKYHI' troposphere-stratosphere-mesosphere general circulation model (GCM) was very sensitive to horizontal resolution (i.e. the fraction of the gravity wave spectrum explicitly resolved), demonstrating a southern winter cold bias of ~70 $^{\circ}$C with ~300 km grid spacing, ~35 $^{\circ}$C with ~100 km grid spacing, and ~10 $^{\circ}$C with ~35 km grid spacing. The lack of convergence at ~100 km grid spacing suggests that simulations performed at climate resolution require the parametrization of drag from the 'missing' gravity waves, i.e. those gravity waves which are not resolved. By contrast, the sensitivity of the cold bias to vertical resolution was shown to be limited. Such biases are particularly evident in the southern winter due to the weak planetary wave driving of the southern winter stratosphere (Shine, 1989; Garcia and Boville, 1994).

In the current IFS, and many other GCMs, the effect of the missing gravity wave drag is parametrized in the simplest possible manner by Rayleigh friction above the stratopause (e.g. McLandress, 1998), which is formulated as a drag force proportional to the mean zonal flow, and which uses a damping coefficient which increases with height. Unfortunately, this does not give a realistic representation of gravity wave drag (e.g. Manzini et al., 1997), and thus the aim of this technical memorandum is to assess the impact of this on the mean circulation and temperature structure. A companion memorandum (Orr, 2009) will discuss the impact of replacing Rayleigh friction with a more physically realistic gravity wave drag parametrization describing the evolution of a broad spectrum of gravity waves emanating from the troposphere. Drag associated with orographic gravity waves, which Boville (1991) showed was important to realistically simulate the northern hemisphere middle atmosphere circulation, is parametrized separately (Palmer et al., 1986).

Recently, Bechtold et al. (2008) showed that the relative southern/northern hemisphere planetary (and synoptic) scale activity of IFS model cycle 32R3 was under/over estimated in 10-day forecasts (based on the 850-hPa temperature forecast anomaly relative to an ECMWF ERA-40 based climatology). This would be

expected to impact significantly on planetary wave driving of the middle atmosphere, however, this was not considered. Moreover, cycle 33R1 included some additional tuning of the convection and diffusion schemes, which is likely to have an indirect effect on planetary wave driving by changing the background environment in which the waves propagate. Thus it is important and necessary to assess the simulation of the middle atmosphere climate in these cycles.

To summarise, therefore, this technical memorandum will assess the middle atmosphere climate of cycles 32R3 and 33R1 of the IFS. 32R3 was operational between 6 November 2007 and 3 June 2008, after which 33R1 became operational. Section 2 describes the simulations and available observations used for validation. Section 3 compares the mean circulation and temperature structure with observations. Focus is on monthly mean results for January and July, as gravity wave forcing is strongest in the southern and northern hemisphere extratropics during winter and summer months. Also investigated is the structure of stationary planetary waves (i.e. waves that do not change in time and whose zonal average is zero) and their eddy forcing of the mean flow, determined by the divergence of the Eliassen-Palm (EP) flux (Andrews et al., 1983). Section 4 presents a discussion and conclusion based on the results.

2. Experiment design

Simulations were conducted at T159L91 (i.e. a horizontal resolution of around 125 km and a model top located at 0.01 hPa). Due to the large inter-annual variability of the atmosphere, particularly in the northern hemisphere, the simulations comprise eight integrations covering years 1994 to 2001, which are then used to evaluate the mean model climate. Each integration is for 13 months, beginning on November 1 of the preceding year (i.e. 1993 to 2000). The integrations are forced at the lower boundary by observed sea-surface temperatures. Mean results based on 24-h intervals are discussed.

The simulations include the Lott and Miller (1997) parametrization of orographic gravity wave drag. In previous cycles, unrealistically large and spurious values of orographic gravity wave drag occurred at the uppermost model levels, partly as a response of the requirement for conservation of momentum forcing, which implies the (artificial) deposition of any remaining gravity wave momentum flux at the model top. The dynamics of the model, in order to maintain balance, strongly compensates. Notably, the zonal and meridional tendencies resulting from the Lott and Miller scheme are currently limited above 50 hPa to 20 m s^{-1} h^{-1}. By linearly depositing the orographic gravity wave momentum flux that remains above 10 hPa, between 10 hPa and the model top, these unrealistic orographic gravity wave drag values and the resulting dynamical response were removed in cycle 32R1. However, it was later found that this resulted in an excessively strong winter jet. Therefore, in 32R3 the height at which the smoothing begins was raised to 0.1 hPa, leaving a substantial amount of orographic gravity wave momentum flux deposited at/above ~1hPa, and thus alleviating the general circulation problem seen. Indeed, orographic gravity waves are typically limited to the troposphere and stratosphere (Eckermann and Preusse, 1999). However, the effect of the smoothing has been re-assessed, and subsequently switched off in the simulations detailed here, as discussed further in section 4.

The results are compared to observations, comprising of ECMWF ERA-Interim (ERAI) reanalysis and the SPARC climatology (Randel et al., 2004). ERAI uses a 12 hour 4D-VAR, T255L60 assimilating model, with a model top of 0.1 hPa. Equivalent January and July mean 8-year fields are computed for the 1994 to 2001

period of the simulations. The SPARC climatology provides a dataset up to a height of 0.01 hPa, from sources such as reanalysis, satellite measurements, rocketsonde wind and temperature data, and lidar temperature measurements. However, there are relatively few measurements directly over the polar regions, and so the climatology effectively stops at 80° north and south, with values at higher latitudes interpolated.

3. Results

3.1 Zonal-mean response of temperature and zonal wind

Figure 1 shows the results for the simulated average January zonal-mean temperature. 32R3 has a northern winter polar low to mid-stratosphere warm bias. While 33R1 is around 10 K colder and similar to the observed value, and shows a warming of the northern winter polar stratopause by around 10 K relative to 32R3. However, both cycles fail to capture the closure of the northern winter polar stratopause. 32R3 and 33R1 southern summer temperatures are largely identical, showing a stratopause warm bias of ~10 K and a southern summer polar upper mesosphere warm bias of ~20 K. The overly warm summer polar upper mesosphere suggests a lack of upwelling, which implies an underestimation of the poleward circulation between the summer and winter hemispheres and weak downwelling over the winter pole, i.e. that the Rayleigh friction forcing of the mean flow is unrealistically weak and underestimates the necessary gravity wave drag. Given realistic descriptions of radiation and planetary waves, the weak downwelling should be associated with a northern winter polar stratosphere cold bias. However, 32R3, and to a lesser extent 33R1, show a warm bias, suggesting that their radiative or planetary wave contributions are themselves biased.

Figure 1 also shows equivalent results for July, which indicate that 32R3 and 33R1 both show a southern winter polar low to mid-stratosphere cold bias of ~10 K. 32R3 and 33R1 northern summer temperatures are largely identical, with both showing a northern summer polar upper mesosphere warm bias of ~20 K. Although this time they are (correctly?) associated with a southern winter polar stratosphere cold bias. This is perhaps partly explained by planetary wave driving having a smaller role in the southern winter hemisphere, meaning that the main processes are radiation and gravity wave drag, leading to the underestimation of gravity wave drag by Rayleigh friction dominating the temperature structure.

Figure 2 summarizes results for the average January zonal-mean zonal wind. The 32R3 northern winter westerly jet has a peak velocity of around 30 m s^{-1}, which is around 10 m s^{-1} less than the observed value. This bias is reduced in 33R1 as the peak velocity of the jet increases to around 40 m s^{-1}. This cycle also captures to a limited extent the observed equatorward tilt of the vortex edge with height. This increase in peak zonal velocity is consistent with the elimination in cycle 33R1 of the northern winter polar stratosphere warm bias (Figure 1) and of the middle atmosphere being in thermal wind balance. By contrast, both cycles show largely identical southern summer easterly winds which are much too weak in the upper mesosphere. This bias is directly related to the use of Rayleigh friction formulated in terms of a damping coefficient which increases with height, and which therefore strongly damps any upper level winds.
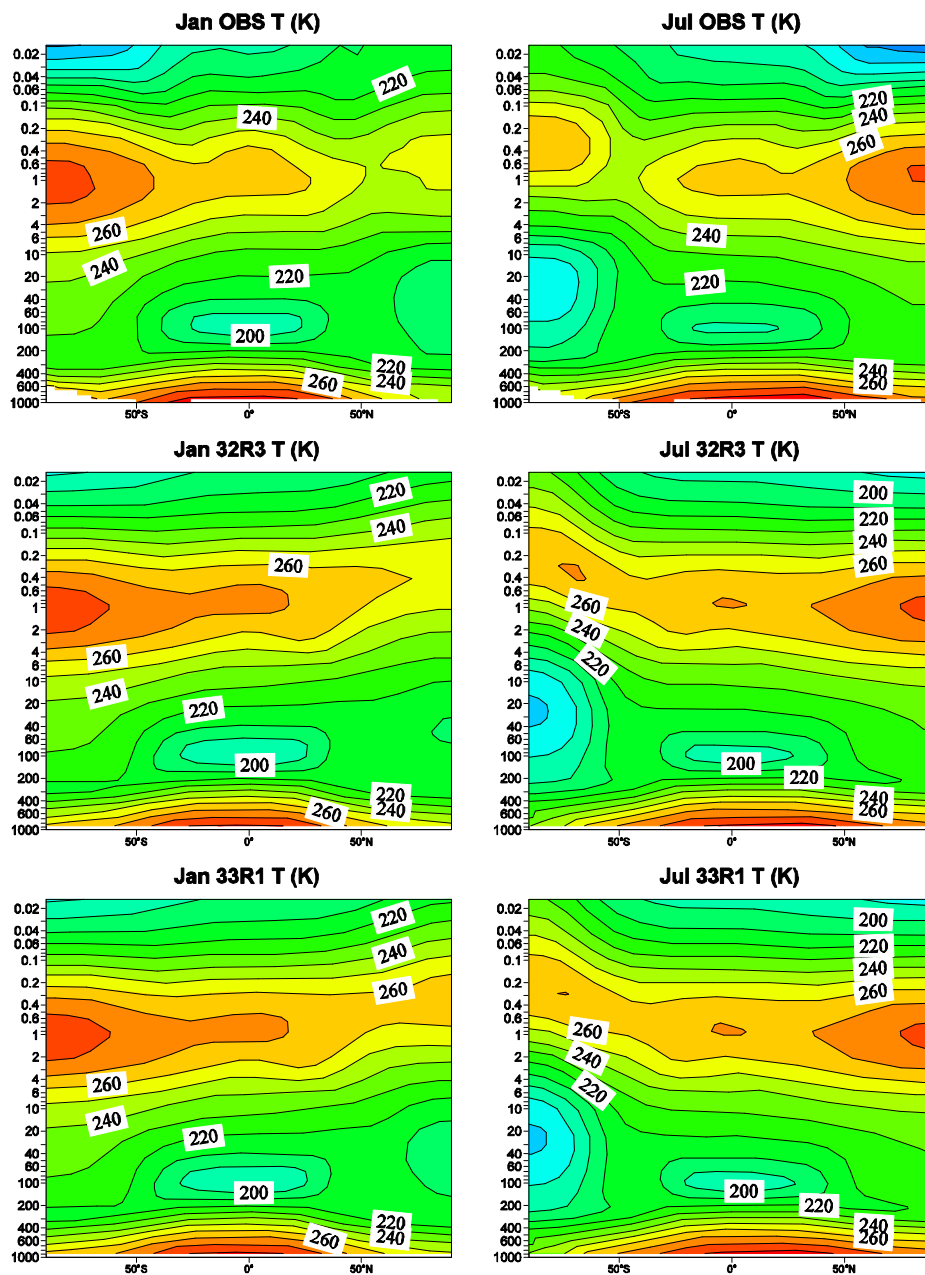
Figure 1: Average January (left) and July (right) cross-sections of zonal-mean temperature for observations (top) and 32R3 (middle) and 33R1 (lower) simulations. The observations are SPARC climatological data. The vertical axis is pressure (hPa) and extends to 0.015 hPa. All simulation results are 8-year averages. SPARC data north of 80°N and south of 80°S is constant and interpolated. The contour interval is 10 K. Warm temperatures are denoted by warm colours.

Equivalent results for July are also shown in Figure 2. As expected, these show a considerably stronger westerly jet in the southern winter. The 32R3 jet has a peak velocity of around 110 m s^{-1}, which compared to the observations is ~30 m s^{-1} too strong. This bias is reduced by around 10 m s^{-1} in 33R1. None of the cycles capture the jets distinct equatorward tilt. The overly strong westerly jet is consistent with the Rayleigh friction underestimating the necessary gravity wave drag. Northern summer easterly winds are too weak in the upper mesosphere.
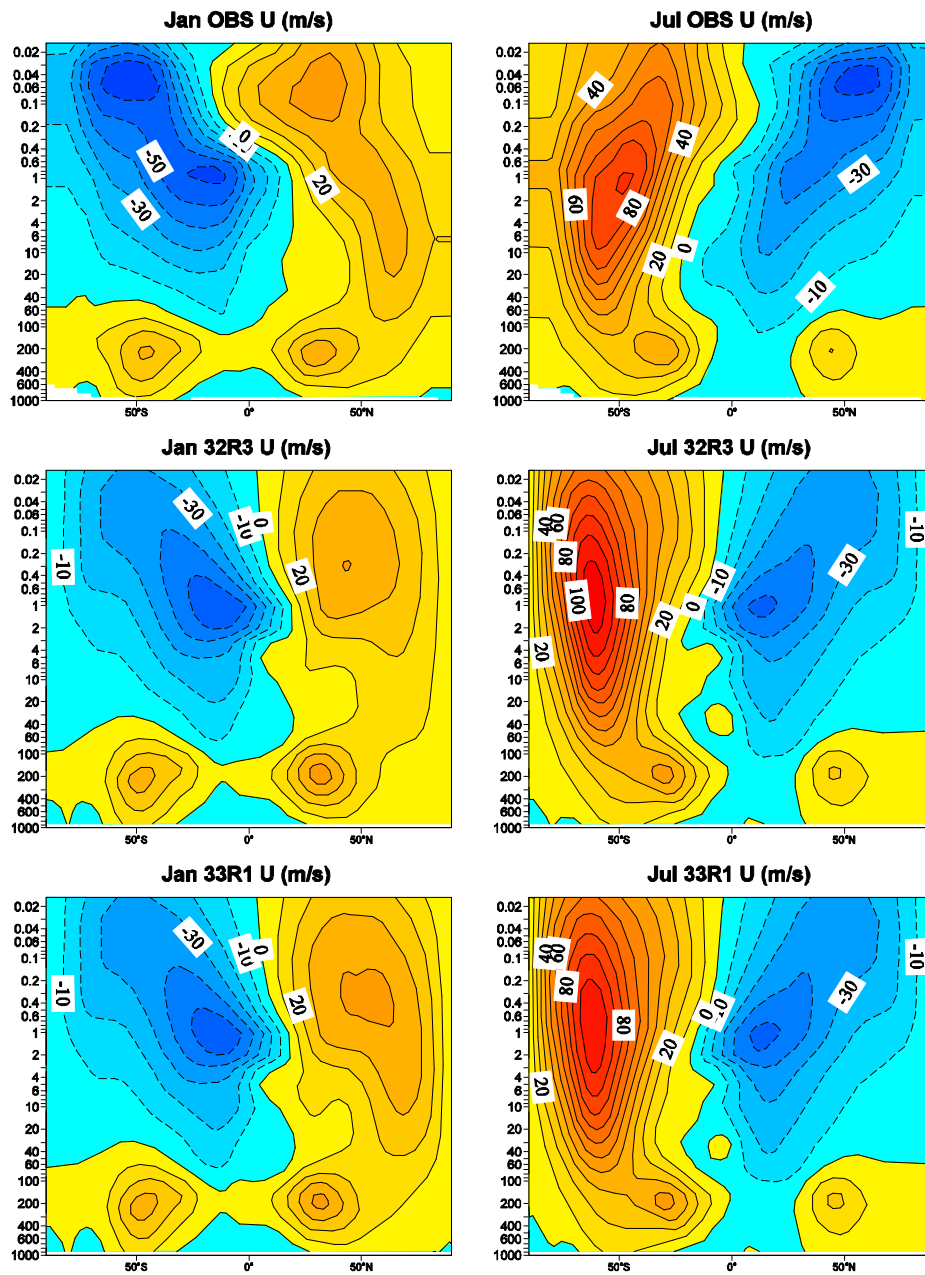
Figure 2: Average January (left) and July (right) cross-sections of zonal-mean zonal wind for observations (upper) and 32R3 (middle) and 33R1 (lower) simulations. The observations are SPARC climatological data. The vertical axis is pressure (hPa) and extends to 0.015 hPa. All simulation results are 8-year averages. SPARC data north of 80°N and south of 80°S is constant and interpolated. The contour interval is 10 m s⁻¹. Easterly winds are denoted by cold colours and dashed contours.

3.2 Planetary waves

Following the approach of Manzini and McFarlane (1998), the average January and July (model resolved) mean stationary planetary wave structure is investigated by examining the zonal velocity amplitude at pressure levels of 100, 10, and 1 hPa (Figure 3). Also computed is the resulting average January and July mean wave EP-flux divergence to examine the wave-driven mean flow acceleration (Figure 4), and which

for stationary waves is dependent on planetary wave dissipation (Holton, 2004). (Note that the EP-flux divergence is divided by $a\cos\varphi$, where a is the earth's radius and φ is the latitude.)

Figure 3 compares the observed and simulated January winter planetary wave amplitudes. Both cycles capture the strength and location of the observed wave at 100 hPa. At 10 hPa the observed wave has a wavenumber 1 signature, which along with the magnitude of the positive velocity region, is broadly captured by the two cycles. By contrast, they, and in particular 32R3, underestimate the magnitude of the negative velocity region, suggesting excessive dissipation. At 1 hPa the observed peak positive and negative velocities both exceed a magnitude of 40 m s^{-1}. This is captured very well by 33R1, but underestimated by a factor of two by 32R3, which again suggests excessive stratospheric dissipation.

The excessive planetary wave dissipation of 32R3 is consistent with it having an overly warm northern winter polar temperature (Figure 1). The relative cooling/warming of the northern winter polar stratosphere/stratopause in 33R1 (Figure 1) is consistent with the reduction in dissipation experienced by this cycle, which implies a decrease in lower stratosphere sinking (i.e. cooling) and upper stratosphere rising (i.e. warming) at the pole (Matsuno and Nakamura, 1979). Moreover, the combination of the good representation of planetary waves in 33R1 and the failure to simulate the expected northern winter polar stratosphere cold bias suggests that the 33R1 radiation scheme is associated with a northern winter polar stratosphere warm bias.

Figure 3 also shows equivalent results for July. Here, the southern winter planetary wave amplitudes are, as expected, considerably smaller than those of the northern winter. Both cycles capture the location of the observed wave at 100 hPa, but slightly overestimate its amplitude. At 10 hPa the observed wave has a wavenumber 1 signature, which is captured by the two cycles. However, 33R1 overestimate its amplitude. At 1 hPa both cycles overestimate the observed peak positive velocity region by a factor of two. Both cycles also strongly overestimate the size of the observed negative velocity region. This suggests insufficient dissipation of the planetary waves in the stratosphere in both cycles.

Figure 4 compares the observed and simulated January stationary wave EP-flux divergence, which is largely easterly (negative) in the stratosphere and mesosphere. The 33R1 northern winter values show a good agreement with observations, which is consistent with it having realistic planetary wave amplitudes (Figure 3). Relative to 32R3, 33R1 shows an increase in westerly (positive) EP-flux divergence throughout the winter polar upper stratosphere and mesosphere, which is perhaps responsible for the strengthening of the westerly jet in 33R1 (Figure 2). Also relative to 32R3, 33R1 shows an increase in easterly EP-flux divergence throughout the mesosphere, consistent with this cycle having a larger planetary wave amplitude at 1 hPa (Figure 3) and thus there being more of the wave to dissipate in this region.

Figure 4 also compares equivalent results for July. These show that both cycles overestimate the EP-flux divergence relative to observations, consistent with the insufficient dissipation in the stratosphere which must be compensated by excessive dissipation in the mesosphere. The increase in EP-flux divergence between 32R3 and 33R1 is smaller than the equivalent northern winter increase discussed above, consistent with there being only small temperature differences between the two cycles in the southern winter (Figure 1). Relative to 32R3, 33R1 shows a small increase in easterly EP-flux divergence at mid-latitudes, which is perhaps responsible for the weakening of the southern winter westerly jet in this cycle (Figure 2).
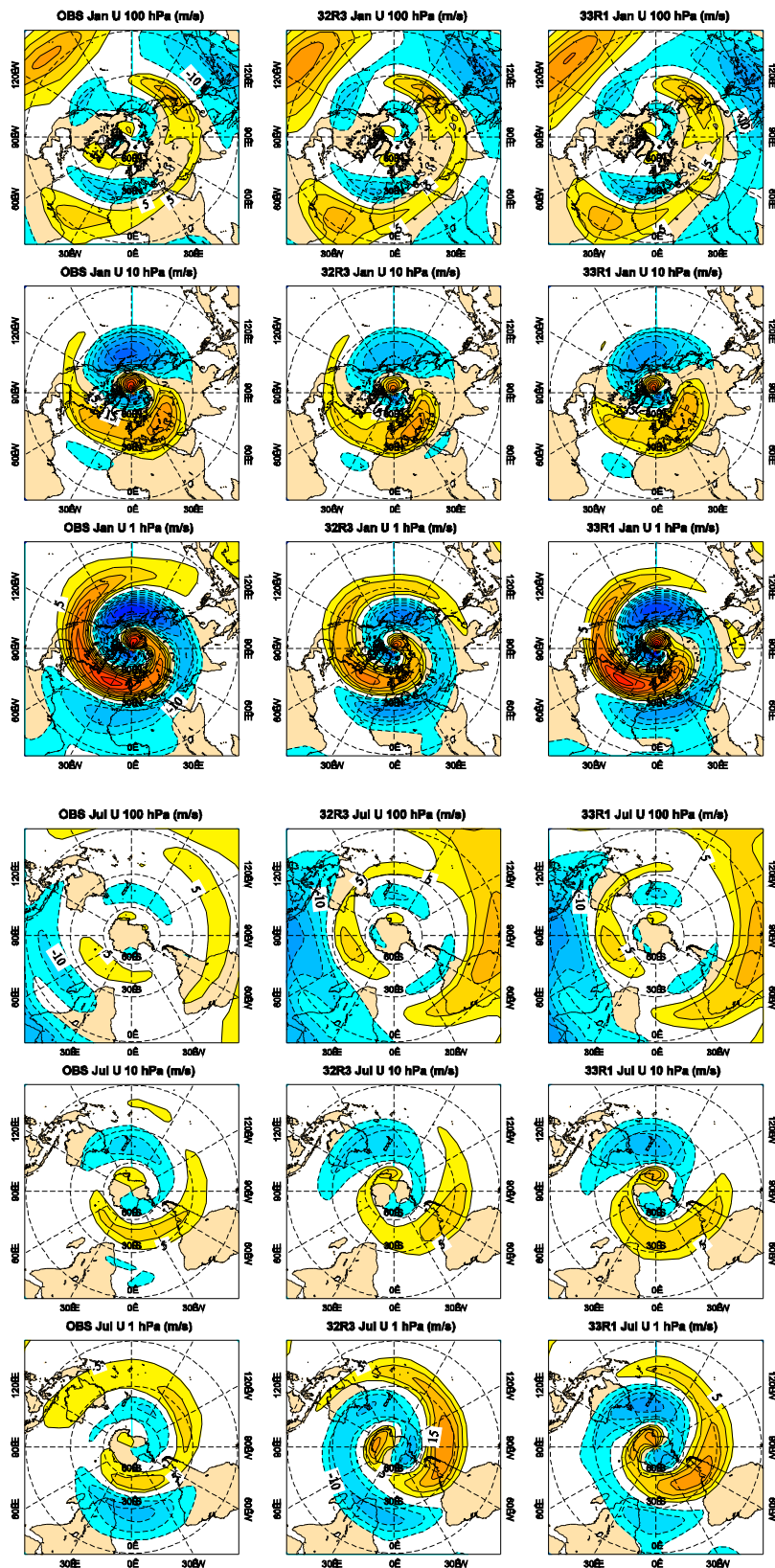
Figure 3: Average January (upper) and July (lower) mean stationary planetary wave zonal wind amplitude (m s^{-1}) at 100 hPa (upper), 10 hPa (middle), and 1 hPa (lower) for observations (left) and 32R3 (centre) and 33R1 (right) simulations. The observations are ERAI data. The simulation results are 8-year averages. The contour interval is ± 5, 10, 15 … 45, 50 m s^{-1}. Negative velocities are denoted by cold colours and dashed contours.
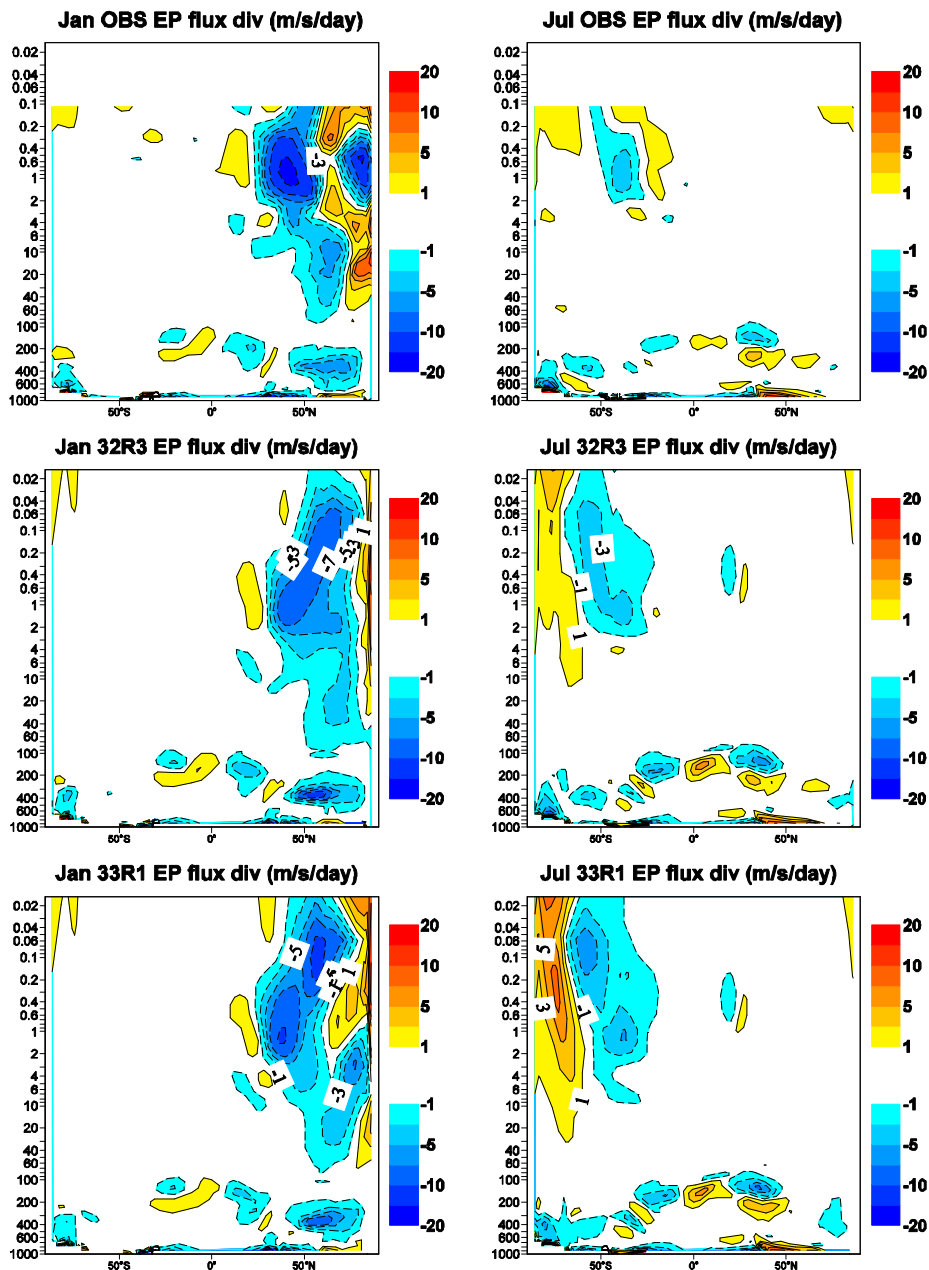
Figure 4: Average January (left) and July (right) cross-sections of zonal-mean stationary wave EP-flux divergence (m s⁻¹ d⁻¹) for observations (top) and 32R3 (middle) and 33R1 (lower) simulations. The observations are ERAI data up to 0.1 hPa. The simulation results are 8-year averages. The vertical axis is pressure (hPa) and extends to 0.015 hPa. The contour interval is ± 1, 3, 5, 7, 10, 15, 20 m s⁻¹ d⁻¹. Easterly forcing of the mean flow is denoted by cold colours and dashed contours.

4.   Discussion and conclusion

The middle atmosphere circulation and temperature structure is largely determined by the balance between the effects of radiative heating and the dissipation of large-scale planetary waves and small-scale non-orographic gravity waves. At climate resolution, non-orographic gravity waves are under or un-resolved, and therefore the gravity wave drag associated with their dissipation in the mesosphere requires parametrization. Prior to and including cycle 33R1, this is crudely achieved with Rayleigh friction. The two cycles examined

here, 32R3 and 33R1, both showed a summer polar upper mesosphere warm bias of ~20 K, which suggests a lack of upwelling, and consequently an underestimation of the poleward circulation between the summer and winter hemispheres and a lack of downwelling over the winter pole, i.e. that the Rayleigh friction underestimates the required gravity wave drag. Given realistic descriptions of radiation and planetary wave activity, therefore, the overly weak downwelling should be associated with too cold winter polar stratospheric temperatures.

However, 32R3 northern winter polar temperatures showed a warm bias (Figure 1). As the middle atmosphere temperature and wind are in thermal balance, this cycle also showed an overly weak winter westerly jet (Figure 2). Boville (1986) demonstrated that with weak background flow, planetary waves are able to penetrate more easily into the stratosphere, and are then deflected poleward rather than equatorward, resulting in enhanced dissipation and stronger wave-mean flow interaction in the lower and middle stratosphere, which maintains the weak winds. This is consistent with 32R3 northern winter planetary wave amplitudes in the stratosphere being too weak (Figure 3). By contrast, a stronger winter jet favours weaker planetary wave driving, consistent with the 33R1 northern winter climate of stronger and more realistic westerlies, and increased and more realistic planetary wave amplitudes. This suggests that the failure to simulate the required northern winter polar cold bias in 33R1 is because the radiation scheme is associated with a northern winter warm bias.

Cycles 32R3 and 33R1 both use the McRAD radiation scheme, which includes the RRTM parametrization of short-wave and long-wave radiation (Morcrette et al., 2007). Iacono et al. (2008) showed that heating rates from high resolution line-by-line radiative transfer models were closely reproduced by the RRTM short-wave and long-wave schemes, with differences of a few hundredths K d^{-1} in the troposphere and a maximum of 0.15 K d^{-1} (around 10%) in long-wave cooling at and just below the stratopause. However, the greenhouse gas (GHG) climatologies of O_3, CO_2, CH_4, N_2O, CFC11, CFC12, CFC22, and CC14 used by the radiation scheme are (with the exception of O_3) constant, and therefore largely unrealistic. Thus a recommendation of this study is that an improved GHG climatology is implemented in the IFS. All simulations show a southern winter polar cold bias, consistent with planetary wave driving having a smaller role in the southern winter hemisphere, and therefore the absence of adequate representation of gravity wave drag dominates the temperature structure.

An improvement on Rayleigh friction is a physically based non-orographic gravity wave parametrization scheme, such as Hines (1997a, b), Warner and McIntyre (2001) and Scinocca (2003). Such schemes require specification of a gravity wave source spectrum, which is typically defined in terms of a broad spectrum of waves of various directions and prescribed horizontal momentum flux, emanating from the troposphere. Typically, the source spectrum is defined to be constant despite observations showing space and time variations (e.g., Fritts and Nastrom, 1992; Allen and Vincent, 1995). However, the (unrealistic) source spectrum is filtered as it propagates through the tropospheric and stratospheric winds, i.e. the intrinsic phase speed of the gravity waves is Doppler shifted as the waves propagate through regions of differing background wind speed, resulting in their absorption. If the background zonal-wind is well captured then the filtering results in a more realistic momentum flux distribution entering the mesosphere (Ern et al., 2004). A companion memorandum investigates the impact on the middle atmosphere climate of cycle 33R1 when Rayleigh friction is replaced by gravity wave forcing using the Scinocca (2003) scheme.
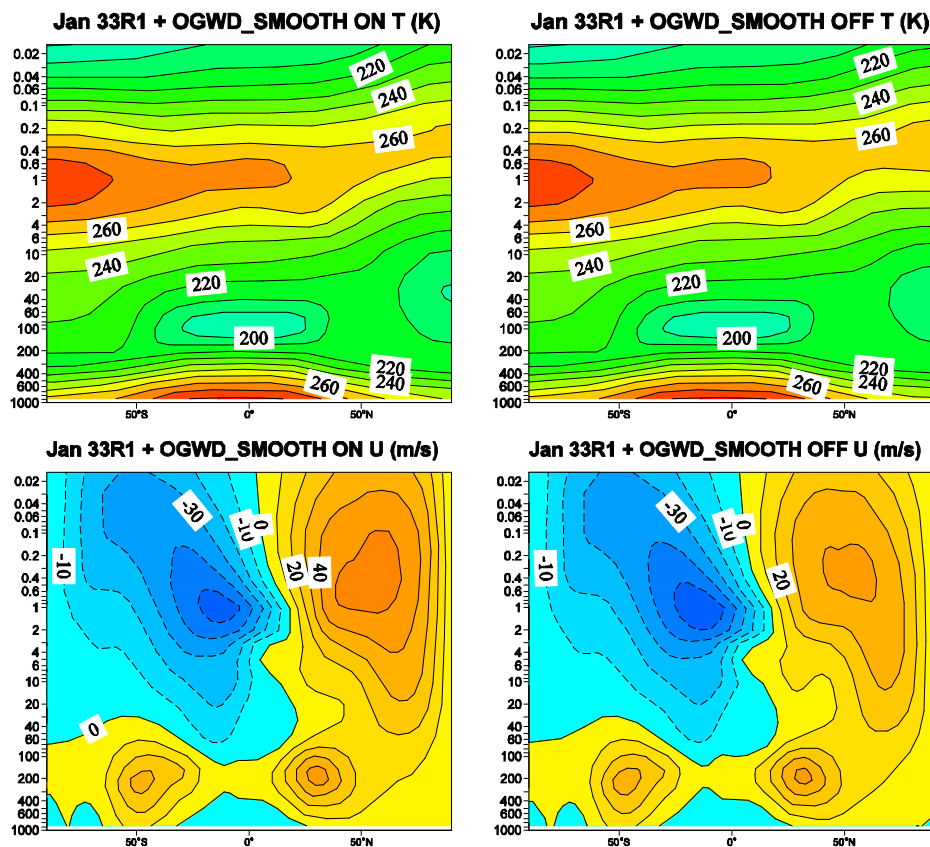
Figure 5: Average January cross-sections of zonal-mean temperature (upper) and zonal velocity (lower) for 33R1 + OGWD_SMOOTH ON (left) and 33R1 + OGWD_SMOOTH OFF (right), where OGWD_SMOOTH ON means that the orographic gravity wave momentum flux at 0.1 hPa is smoothed between 0.1 and 0.01 hPa. All simulation results are 8-year averages. The vertical axis is pressure (hPa) and extends to 0.015 hPa. The contour intervals are 10 K and 10 m s⁻¹. Easterly winds are denoted by cold colours and dashed contours. Warm temperatures are denoted by warm colours.

Finally, to illustrate the impact of the orographic gravity wave drag (OGWD) smoothing, the 33R1 simulation was re-run with the smoothing from 0.1 hPa switched on, referred to as 33R1 + OGWD_SMOOTH ON. Figure 5 compares the resulting average January zonal-mean temperature and zonal velocity with the results of 33R1, which had the smoothing switched off. These have been labelled 33R1 + OGWD_SMOOTH OFF, and are the results shown previously in Figures 1 and 2. It is apparent that the 33R1 + OGWD_SMOOTH ON simulation results in a cooling of the northern winter polar stratosphere and stratopause and a significant strengthening of the winter westerly jet. The cooling may be understood from a reduction in orographic gravity wave drag in the winter midlatitude mesosphere due to less orographic gravity wave momentum flux being deposited above 0.1 hPa with smoothing on (not shown), which is consistent with the much stronger winter jet in the mesosphere generating an additional Coriolis torque which modulates the meridional circulation by reducing the summer pole to winter pole drift, and reducing sinking over the pole. Southern hemisphere winter results showed negligible difference between the two simulations (not shown), consistent with the comparative lack of orography and consequent small values of orographic gravity wave drag in the southern hemisphere. Thus, given the clear improvement in northern winter temperature structure and circulation, a recommendation of this study is that the smoothing is removed from cycle 33R1 of the IFS.
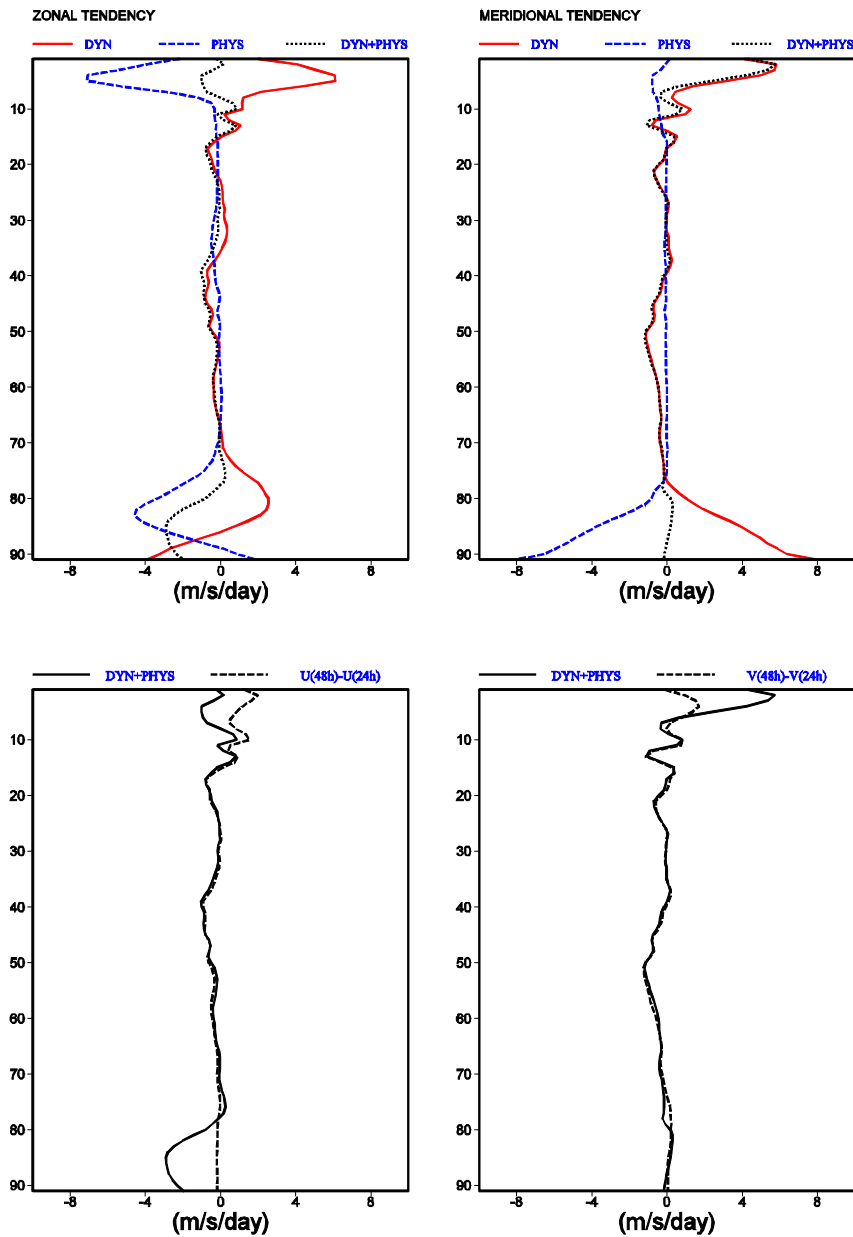
Figure 6: Area-averaged profiles of zonal (left) and meridional (right) tendencies. The upper panels compare dynamical (DYN), physical (PHYS), and total (DYN+PHYS) accumulated tendencies between T+24 h and T+48 h from a T159L91 33R1 + CLIM_GHG + OGWD_SMOOTH OFF simulation, beginning 1 November 2000. The area-average is 40 to 70°N, and 160°E to 160°W, i.e. northern hemisphere mid-latitude land. The vertical axis is model level. The lower panels compare the total (DYN+PHYS) tendency with the actual horizontal wind difference U, V (T+48 h) - U, V (T+24 h), where U, V is the zonal, meridional velocity. PHYS only contains contributions from orographic gravity wave drag, which is the dominant contribution at the model top, and vertical diffusion.

However, despite this improvement, Figure 6 shows that the resulting increase in orographic gravity wave momentum flux deposited above 0.1 hPa when the smoothing is off produces large, unrealistic area-averaged zonal and meridional orographic gravity wave tendencies at the model top. Here, the area-average is over northern hemisphere mid-latitude land. At the top of the model, the tendencies from the model physics are

dominated by orographic gravity wave drag. Also evident is the strong compensation from the dynamics. Moreover, a comparison of the total tendencies (i.e. dynamics + physics) with the resulting horizontal wind tendencies (also Figure 6) indicates a significant difference above model level 10 (i.e. around 1 hPa) due to the semi-implicit solution procedure, which points towards a large imbalance near the model top.

A (more realistic) reduction in momentum deposition at the model top and consequent alleviation of this imbalance and the need for smoothing would be achieved by earlier (lower down) orographic wave breaking, which is assisted by improved closure of the winter westerly jet, i.e. weaker zonal-winds (Palmer et al., 1986) at the model top. Such a jet closure is achieved once a more physically realistic non-orographic gravity wave drag scheme replaces Rayleigh friction (e.g. Scinocca, 2003; Orr, 2009).

Acknowledgements

References

Allen, S. J., and R. A. Vincent, 'Gravity wave activity in the lower atmosphere: Seasonal and latitudinal variations', *J. Geophys. Res.*, **100**, pp. 1327-1350, 1995.

Andrews, D. G., J. D. Mahlman, and R. W. Sinclair, 'Eliassen-Palm diagnostics of wave-mean flow interaction in the GFDL "SKYHI" general circulation model', *J. Atmos. Sci.*, **40**, pp. 2768-2784, 1983.

Andrews, D. G., J. R. Holton, and C. B Leovy, *Middle Atmosphere Dynamics*, International Geophysical Series, Vol. 40, 489 pp., 1987.

Bechtold, B., M. Kohler, T. Jung, F. Doblas-Reyes, M. Leutbecher, M. Rodwell, F. Vitart, and G. Balsamo, 'Advances in simulating atmospheric variability the ECMWF model: From synoptic to decadal time-scales', *Q. J. R. Met. Soc.*, **134**, pp. 1337-1351, 2008.

Boville, B. A., 'Wave mean flow interactions in a general circulation model of the troposphere and stratosphere', *J. Atmos. Sci.*, **43**, pp. 1711-1144, 1986.

Boville, B. A., 'Sensitivity of the simulated climate to model resolution', *J. Climate*, **4**, pp. 469-485, 1991.

Cariolle, D., M. J. Evans, M. P. Chipperfield, N. Butkovskaya, A. Kukui, and G. Le Bras, 'Impact of the new HNO_3-forming channel of the HO_2+NO reaction on tropospheric HNO_3, NO_x, HO_x and ozone', *Atmos. Chem. Phys.*, **8**, pp. 4061-4068, 2008.

Eckermann, S. D., and P. Preusse, 'Global measurements of stratospheric mountain waves from space', Science, **286**, pp. 1534-1537, 1999.

Ern, M., P. Preusse, M. J. Alexander, and C. D. Warner, 'Absolute values of gravity wave momentum flux derived from satellite data', *J. Geophys. Res.*, **109**, D20103, doi:10.1029/2004JD004752, 2004.

Fritts, D. C., and G. D. Nastrom, 'Sources of mesoscale variability of gravity waves. Part II: frontal, convective, and jet stream excitation', *J. Atmos. Sci.*, **49**, pp. 111-127, 1992.

Garcia, R. R., and S. Solomon, 'The effect of breaking gravity waves on the dynamics and chemical composition of the mesosphere and lower thermosphere', *J. Geo. Res.*, **90,** pp. 3850-3868, 1985.

Garcia, R. R., and B. A. Boville, ' "Downward Control" of the mean meridional circulation and temperature distribution of the polar winter stratosphere', *J. Atmos. Sci.*, **51**, pp. 2238-2245, 1994.

Gardner, C. S., M. S. Miller, and C. H. Liu, 'Rayleigh lidar observations of gravity wave activity in the upper stratosphere at Urbana, Illinois', *J. Atmos. Sci.*, **46**, pp. 1838-1854, 1989.

Hamilton, K., R. J. Wilson, J. D. Mahlman, and L. J. Umscheid, 'Climatology of the SKYHI troposphere-stratosphere-mesosphere general circulation model', *J. Atmos. Sci.*, **52**, pp. 5-42, 1995.

Hamilton, K., R. J. Wilson, and R. S. Hemler, 'Middle atmosphere simulated with high vertical and horizontal resolution versions of a GCM: Improvements in the cold pole bias and generation of a QBO-like oscillation in the tropics', *J. Atmos. Sci.*, **56**, pp. 3829-3846, 1999.

Hines, C. O., 'Doppler spread parameterization of gravity wave momentum deposition in the middle atmosphere. Part 1: Basic formulation', *J. Atmos., Solar Terr., Phys.*, **59**, pp. 371-386, 1997a.

Hines, C. O., 'Doppler spread parameterization of gravity wave momentum deposition in the middle atmosphere. Part 2: Broad and quasi monochromatic spectra and implementation', *J. Atmos., Solar Terr., Phys.*, **59**, pp. 387-400, 1997b.

Holton, J. R., 'The role of gravity wave induced drag and diffusion in the momentum budget of the mesosphere', *J. Atmos. Sci.*, **39**, pp. 791-799, 1982.

Holton, J. R., 'The influence of gravity wave breaking on the general circulation of the middle atmosphere', *J. Atmos. Sci.*, **40**, pp. 2497-2507, 1983.

Holton, J. R., *An introduction to dynamic meteorology*, Elsevier/Academic Press, fourth edition, 535 pp., 2004.

Iacono, M. J., J. S. Delamere, E. J. Mlawer, and M. W. Shephard, 'Radiative forcing by long-lived greenhouse gases: Calculations with the AER radiative transfer models', *J. Geophys. Res.*, **113**, D13103, doi:10.1029/2008JD009944, 2008.

Kanzawa, H., 'Warm stratopause in the Antarctic winter', *J. Atmos. Phys.,* **46**, pp. 435-438, 1989.

Lott, F. L., and M. Miller, 'A new subgrid scale orographic drag parametrization; its formulation and testing', *Q. J. R. Met. Soc.*, **123**, pp. 101-127, 1997.

Manzini, E., N. A. McFarlane, and C. McLandress, 'Impact of the Doppler spread parameterization on the simulation of the middle atmosphere circulation using the MA/ECHAM4 general circulation model', *J. Geophys. Res.*, **102**, pp. 25751-25762, 1997.

Manzini, E., and N. A. McFarlane, 'The effect of varying the source spectrum of a gravity wave parameterization in a middle atmosphere general circulation model', *J. Geophys. Res.*, **103**, pp. 31523-31539, 1998.

Matsuno, T., and K. Nakamura, 'The eulerian- and lagrangian-mean meridional circulations in the stratosphere at the time of a sudden warming', *J. Atmos. Phys*., **36**, pp. 640-654, 1979.

McLandress, C., 'On the importance of gravity waves in the middle atmosphere and their parameterization in general circulation models', *J. Atmos. Sol. Terr. Phys.*, **60**, pp. 1357-1383, 1998.

Morcrette, J.-J., and co-authors, 'Recent advances in radiation transfer parameterizations', ECMWF Technical Memorandum, No. 539, 2007.

Orr, A., 'The representation of non-orographic gravity waves in the IFS. Part II: A physically based spectral parametrization', ECMWF Technical Memorandum, No. 593, 2009.

Palmer, T. N., G. J. Shutts, and R. Swinbank, 'Alleviation of a systematic westerly bias in general circulation and numerical weather prediction models through an orographic gravity wave drag parameterization', *Q. J. R. Met. Soc.*, **112**, pp. 1001-1039, 1986.

Randel, W. J., and co-authors, 'The SPARC intercomparison of middle atmosphere climatologies', *J. Climate*, **17**, pp. 986-1003, 2004.

Scinocca, J. F., 'An accurate spectral nonorographic gravity wave drag parameterization for general circulation models', *J. Atmos. Phys*., **60**, pp. 667-682, 2003.

Shine, K., 'Sources and sinks of zonal momentum in the middle atmosphere diagnosed using the diabatic circulation', *Q. J. R. Met. Soc.*, **115**, pp. 265-292, 1989.

Warner, C. D., and M. E. McIntyre, 'An ultra-simple spectral parameterization for non-orographic gravity waves', *J. Atmos. Sci.*, **58**, pp. 1837-1857, 2001.